Tellus (1995), 47B, 281–300
Printed in Belgium – all rights reserved

TELLUS
ISSN 0280–6509

The sulfate-CCN-cloud albedo effect

A sensitivity study with two general circulation models

By OLIVIER BOUCHER*, *Laboratoire de Météorologie Dynamique du CNRS, Ecole Normale Supérieure, 24 rue Lhomond, 75231 Paris Cedex 05, France* and ULRIKE LOHMANN, *Max-Planck-Institute for Meteorology, Bundesstrasse 55, 20146 Hamburg, Germany*

(Manuscript received 9 June 1994; in final form 14 October 1994)

ABSTRACT

Aerosol particles, such as sulfate aerosols, can act as cloud condensation nuclei (CCN). The CCN spectrum and the water vapor supply in a cloud determine the cloud droplet number concentration (CDNC) and hence the shortwave optical properties of low-level liquid clouds. The capability of anthropogenic aerosols to increase cloud reflectivity and thereby cool the Earth's surface is referred to as the indirect effect of anthropogenic aerosols. To obtain an estimate of this effect on climate, we empirically relate the CDNC, and thus the cloud optical properties, of two general circulation models (GCM) to the sulfate aerosol mass concentration derived from a chemical transport model. Based on a series of model experiments, the normalized globally-averaged indirect forcing is about -1 W m^{-2} and ranges from -0.5 to -1.5 W m^{-2} in both GCMs for different experiments. However, it is argued that the total uncertainty of the forcing is certainly larger than this range. The overall agreement between the two climate models is good, although the geographical distributions of the forcing are somewhat different. The highest forcings occur in and off the coasts of the polluted regions of the Northern Hemisphere. The regional distribution of the forcing and the land/sea constrast are very sensitive to the choice of the CDNC-sulfate mass relationship. The general patterns of the forcing, and the appropriateness of the different CDNC-sulfate mass relationships, are assessed. We also examine the simulated droplet effective radii and compare them with satellite retrievals.

1. Introduction

Anthropogenic aerosols are thought to have two potential effects on climate. In clear-sky conditions they scatter solar radiation back to space, reducing solar irradiance at the ground. This effect is usually called the direct effect and its magnitude has recently been estimated by several authors to range from -0.3 to -1 W m^{-2} (Charlson et al., 1990, 1991 and 1992; Kiehl and Briegleb, 1993). The direct effect can partly offset the warming expected from increasing levels of greenhouse gases, although the characteristics of the aerosol and greenhouse forcings are different (Wigley, 1989; IPCC, 1992; Taylor and Penner, 1994). Anthropogenic aerosols, such as sulfate particles, can also act as cloud condensation nuclei (CCN). The number of available CCN is one of the parameters that determines the cloud droplet number concentration (CDNC), cloud albedo and development of precipitation (Albrecht, 1989; Fouquart and Isaka, 1992). An increase in CCN, for a constant liquid water content, leads to a larger concentration of cloud droplets of smaller radius, thus increasing cloud reflectivity (Twomey, 1974; Twomey et al., 1984). This second effect is referred to as the indirect effect. The resulting forcing is also negative and adds to the direct effect, but it is by far more uncertain, because the involved microphysical processes are not well understood (Penner et al., 1994). However, some evidence shows that this forcing can be substantial. Shiptrack observations reported by Coakley et al. (1987), Radke et al. (1989) and King et al. (1993) reveal a simultaneous decrease in cloud droplet

* Corresponding author.

radii and increase in cloud albedo. Falkowski et al. (1992) and Kim and Cess (1993) reported enhanced cloud albedo off the east coasts of industrialized regions.

Attempts to estimate the magnitude of the indirect effect include works of Charlson et al. (1992), Schwartz (1988) and Schlesinger et al. (1992). Chuang et al. (1994) used a climate model coupled with a 3-D chemical transport model to simulate the global sulfur cycle and estimate both direct and indirect forcings of anthropogenic sulfate aerosols. They make the assumption of a background aerosol size distribution which is modified either by condensation of gas-phase sulfuric acid or aqueous-phase oxidation of sulfur dioxide (SO_2) followed by evaporation of droplets, the respective importance of these two transformations being fixed. The CDNC is then parameterized in terms of the aerosol size distribution and vertical velocity and is used to compute cloud albedo. The simulated indirect radiative forcing is about -0.5 W m^{-2} but the authors point out that this estimate is uncertain. Boucher and Rodhe (1994), and Jones et al. (1994), used a different approach and related the sulfate aerosol mass concentration of a chemical transport model to CDNC through empirically-derived relationships. The forcing due to enhanced low-level cloud albedo was found to be significant in both studies but very dependent on the assumed relationship in the study of Boucher and Rodhe (1994).

In the present study, we similarly relate CDNC to the sulfate aerosol mass of a chemical transport model (and, in turn, droplet effective radius to CDNC) to estimate the climatic effect of the potential man-made cloud brightening. Special emphasis is placed on the uncertainties of this approach, which is estimated through the use of several CDNC-sulfate mass relationships, including a maximum and a minimum envelope of the available data. The specificity of the present study also lies in the comparison of results coming from two climate models with different parameterizations of moist processes and cloud optical properties. Before describing our experiments, we assess the inherent difficulties of modelling the indirect effect. The results are then discussed and assessed in view of the simulated cloud droplet radii. A comparison with previous estimates and a discussion of remaining uncertainties are also presented.

2. Modelling the indirect effect of sulfate aerosol particles

2.1. Factors influencing the cloud droplet number concentration

At the present time, CDNC cannot be computed in a realistic way in large-scale models because it varies over a large range and depends on several factors that are not easy to predict, such as subgrid-scale updraft velocity and maximum supersaturation in clouds. The problem of relating CDNC to aerosol mass (and specifically sulfate) may be divided into two steps:

(i) *Relating the CCN concentration to the sulfate aerosol mass.* There is a large uncertainty in relating aerosol (and CCN) number concentration to sulfate mass concentration because the relative importance of the different pathways of SO_2 oxidation are not well understood. SO_2 can be oxidized into sulfuric acid in the gas-phase, which in turn can either condense onto existing particles or form new particles by homogeneous nucleation. Formation of new particles is difficult to predict since it decreases as the total area of pre-existing aerosol particles increases (Clarke, 1992; Charlson, 1992). But a large fraction of SO_2 is thought to be oxidized in the liquid-phase of cloud droplets, causing the initial cloud droplet nuclei to grow when the droplet evaporates but leaving unchanged the total aerosol number concentration (Hegg et al., 1980). Using the chemical transport model MOGUNTIA, Langner et al. (1992) estimated that 44% of anthropogenic SO_2 emissions is transformed through in-cloud oxidation and is associated with pre-existing particles and at most 6% is available for formation of new particles. However, a more detailed model is needed to quantify the respective fractions of SO_2 that are incorporated into pre-existing particles or used to create new particles. As argued by Leaitch and Isaac (1994) "6% of the anthropogenic sulfur could produce a very large number of sulfate particles depending on their size". Kaufman and Tanré (1994) showed that these small new particles could also be activated in stratiform clouds if one considers the natural variability of even low-average supersaturations. Also, the sulfate mass added to already existing particles can shift the aerosol size distribution towards larger radii, which would then increase the number of available CCN (Hegg et al., 1980).

(ii) *Relating CDNC to the concentration of CCN.* The number of activated CCN (i.e., CDNC) results from a competition between the amount of available water vapor and the consumption of water vapor by condensation on CCN (e.g., Hobbs, 1993). This number of activated CCN depends non-linearly on the updraft velocity (Gillani et al., 1992), the total aerosol number, their size distribution and chemical composition (e.g., the respective amounts of soluble and insoluble materials) (Graßl, 1988).

The number of activated CCN may not increase linearly with the number of CCN. There is a saturation effect linked with the fact that enhanced concentrations of CCN diminish the supersaturation, impeding the activation of more CCN. Gillani et al. (1992) observed that the activated fraction of accumulation-mode particles in a cloud is close to unity for low total concentrations of these particles but decreases as their total number increases. The transition between these two regimes depends on the meteorological conditions but occurred at particle loadings of about 600 to 800 cm^{-3} for the continental stratiform clouds considered in their study.

2.2. *Relationship between CDNC and sulfate mass concentration*

Considering the difficulties mentioned above, we empirically relate CDNC to the mass concentration of sulfate particles, determined from the chemical transport model MOGUNTIA, for present-day and pre-industrial conditions, respectively. The existence of a relationship between aerosol mass and CDNC number is questionable for two reasons. First, aerosol mass and number concentrations lie in different modes or size ranges of CCN (Hallberg, 1994; Anderson et al., 1994). Secondly, the lifetime of CCN mass concentration is longer than that of CCN number concentration, because there are more sinks for the CCN number concentration (Ackerman et al., 1994; Charlson, 1992). Nevertheless, despite a large scatter in the data, the existing measurements show a general increase of CDNC with rising aerosol mass, sufficiently correlated to derive a relationship.

We consider for this purpose the following datasets.

(a) Leaitch et al. (1992a, 1992b) measured simultaneously CDNC and cloud water sulfate for stratiform and cumuliform clouds (see Figs. 1b, c, d). They present 85 compressed samples, obtained during flights over North America performed under different conditions and seasons. The uncertainty in CDNC is estimated to be $\pm 10\%$. Together with a large variability in CDNC, there is a covariation of CDNC and cloud water sulfate concentration and the authors give a relationship between them. The problem thus arises to tie the concentration of cloud water sulfate to that of atmospheric sulfate mass, which will depend on the sulfate scavenging efficiency and in-cloud oxidation of SO_2. Since in-cloud oxidation of SO_2 is accounted for in MOGUNTIA, we need to obtain only the sulfate scavenging efficiency which is highly variable. It has been measured to be 30% to 90% by different authors (Hallberg et al., 1995; Hegg and Hobbs, 1988; ten Brink et al., 1987; Hegg et al., 1984; Sievering et al., 1984). We assume that 60% of the sulfate mass is taken up by coud droplets, which lies in the average of these measurements. The results are almost insensitive to this assumption because of the sublinear character of the sulfate mass to CDNC relationship.

(b) Berresheim et al. (1993) and Quinn et al. (1993) presented simultaneous measurements of non-sea-salt sulfate (nss sulfate) and CCN active at 0.3% supersaturation at Cheeka Peak, which is located in Washington State, USA, approximately 2 km inland from the Pacific Ocean (see Figs. 1a, d). A strong correlation was observed between CCN at 0.3% and nss sulfate mass concentration for the 11 data points of Berresheim et al. (1993). The data from Quinn et al. (1993) suggest a steeper regression line between CCN and aerosol mass concentration, but this results from only four long-term averaged data pairs.

(c) Hegg et al. (1993) measured DMS, nss sulfate mass and CCN active at different supersaturations over the Northeast Atlantic under very different conditions leading to a large range of mass concentrations for the sulfate mass and suggesting an anthropogenic influence on some days (see Figs. 1a, d). They found a significant correlation between sulfate aerosol mass and CCN concentration but concluded that other chemical species also played a role in the formation of CCN during the time of their experiments. We compute CCN concentrations active at 0.3% supersatura-

tion ($S = 0.3$) using the following equation (Twomey, 1959):

$$\mathrm{CCN}(S) = c\, S^k, \tag{1}$$

where c, the CCN concentration active at 1% supersaturation, and k, the slope parameter, are given in the experimental data.

For the datasets described in (b) and (c) we assume that the CCN concentration at 0.3% supersaturation equals the number of cloud droplets. There is little experimental data to support this assumption but the supersaturation peak in maritime stratiform is usually in the range 0.1 to 0.3% (e.g., Albrecht et al., 1988). Also, considering the natural variability in CCN concentrations, the rough agreement that we obtain between the different experimental studies (see Fig. 1a) supports a posteriori that this assumption is reasonable for maritime stratiform clouds.

(d) Van Dingenen et al. (Van Dingenen, unpublished data) measured aerosol size distribution and sulfate mass concentration over the North Atlantic. They identified accumulation-mode particles (AMP) to be cloud droplet residue particles (Hoppel et al., 1986, 1990). Gillani et al. (1992) report high aerosol activation efficiency for AMP concentrations below 600 cm^{-3}, which is the case here. Therefore, we consider that the AMP concentration is a good indicator of CDNC, although some cloud droplet residue particles can be found in the nucleation mode (Anderson et al., 1994; Gillani et al., 1992). Their data span a large range of sulfate concentrations (see Figs. 1a, d).

The data from these five experimental studies are summarized in Table 1 and plotted in Fig. 1.

We extract 4 possible relationships between CDNC and sulfate mass concentration. A log–log representation of the data and log–log regression

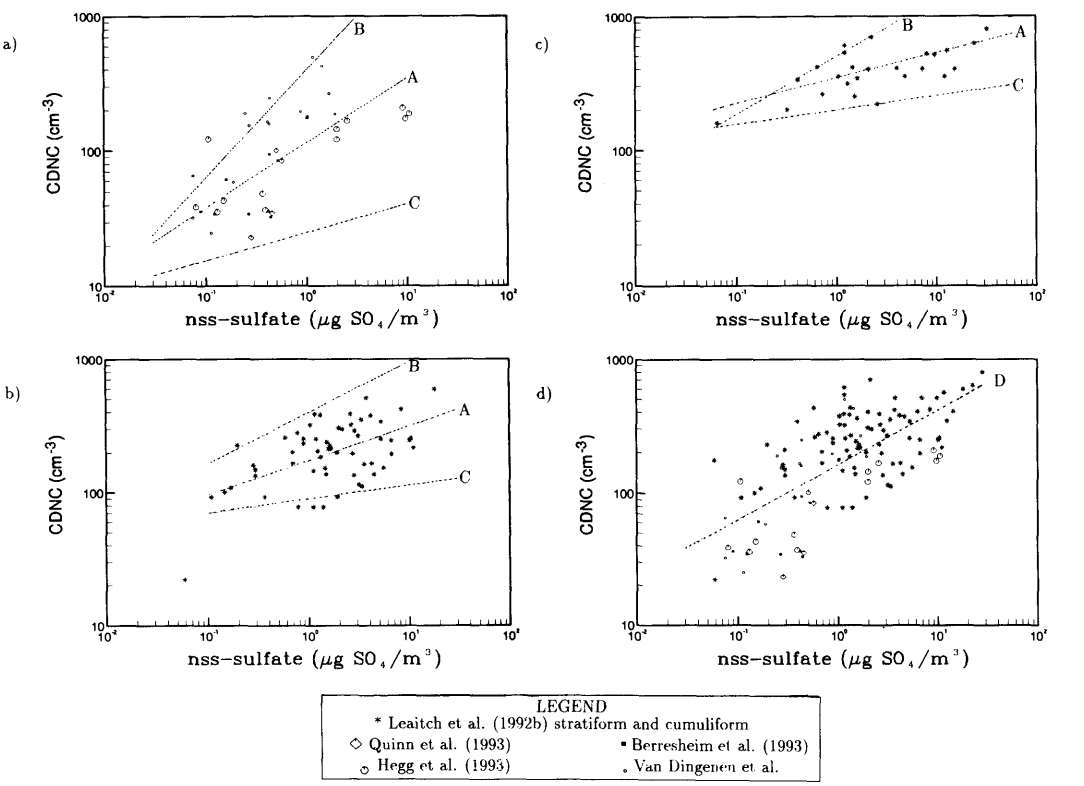

Fig. 1. Cloud droplet number concentration as a function of sulfate aerosol mass concentration for (a) maritime clouds, (b) continental stratiform clouds, (c) continental cumuliform clouds, and (d) all data. The regression lines are numbered as in the text.

Table 1. *Summary of the measurements used in this study*

Ref.	No. data pairs	Location	Measured quantities and assumptions
Berresheim et al. (1993)	11	NE Pacific	sulfate aerosol mass and CCN at 0.3 % S_{max} CCN concentration at 0.3 % S_{max} is CDNC
Quinn et al. (1993)	4	NE Pacific	sulfate aerosol mass and CCN at 0.3 % S_{max} CCN concentration at 0.3 % S_{max} is CDNC
Hegg et al. (1993)	12	NE Atlantic	sulfate aerosol mass and CCN at 0.2 to 2.0 % S_{max} CCN concentration at 0.3 % S_{max} is CDNC
Van Dingenen et al.	14	N Atlantic	sulfate aerosol mass and aerosol size distribution accumulation-mode particle concentration is CDNC
Leaitch et al. (1992b)	59 St 26 Cu	NE America	cloud water sulfate and CDNC 60 % of the sulfate aerosol mass are scavenged by clouds

lines have been preferred because it allows a better representation of low sulfate aerosol concentrations. The first relationship that we derive consists of separate least-square fits for maritime and continental clouds, with continental stratiform clouds distinguished from the convective ones for the ECHAM model (see below) only, (relationship A, see Figs. 1a, b, c):

$$\left.\begin{aligned} \mathrm{CDNC}^{\mathrm{St}}_{\mathrm{cont}} &= 10^{2.24 + 0.257 \log(m_{\mathrm{SO_4}})} \\ \mathrm{CDNC}^{\mathrm{Cu}}_{\mathrm{cont}} &= 10^{2.54 + 0.186 \log(m_{\mathrm{SO_4}})} \\ \mathrm{CDNC}_{\mathrm{ocean}} &= 10^{2.06 + 0.48 \log(m_{\mathrm{SO_4}})} \end{aligned}\right\} \quad (A)$$

where $m_{\mathrm{SO_4}}$ is expressed in $\mu\mathrm{g\,SO_4\,m^{-3}}$ and CDNC in $\mathrm{cm^{-3}}$.

In addition, we derive two more relationships B and C (see Figs. 1a, b, c) with expressions:

$$\left.\begin{aligned} \mathrm{CDNC}^{\mathrm{St}}_{\mathrm{cont}} &= 10^{2.6 + 0.38 \log(m_{\mathrm{SO_4}})} \\ \mathrm{CDNC}^{\mathrm{Cu}}_{\mathrm{cont}} &= 10^{2.7 + 0.43 \log(m_{\mathrm{SO_4}})} \\ \mathrm{CDNC}_{\mathrm{ocean}} &= 10^{2.6 + 0.80 \log(m_{\mathrm{SO_4}})} \end{aligned}\right\} \quad (B)$$

$$\left.\begin{aligned} \mathrm{CDNC}^{\mathrm{St}}_{\mathrm{cont}} &= 10^{1.95 + 0.105 \log(m_{\mathrm{SO_4}})} \\ \mathrm{CDNC}^{\mathrm{Cu}}_{\mathrm{cont}} &= 10^{2.3 + 0.105 \log(m_{\mathrm{SO_4}})} \\ \mathrm{CDNC}_{\mathrm{ocean}} &= 10^{1.4 + 0.21 \log(m_{\mathrm{SO_4}})} \end{aligned}\right\} \quad (C)$$

These relationships have been chosen so that their slopes are maximum and minimum and so that they provide an upper and a lower envelope to all the data points.

Finally, one can fit all the datasets to a single relationship D which we choose again to be a log–log regression line (see Fig. 1d):

$$\mathrm{CDNC} = 10^{2.21 + 0.41 \log(m_{\mathrm{SO_4}})}. \quad (D)$$

It is important to note that these relationships are strongly sublinear: for instance a twofold increase in $m_{\mathrm{SO_4}}$ leads to a 33 % increase in CDNC for relationship D. Hegg (1994) obtained as well sublinear relationships between sulfate mass and CCN concentration.

2.3. *Droplet effective radius*

The next step is to relate CDNC to the droplet effective radius, r_e, which is a key parameter to determine shortwave radiative properties of clouds (see next section). The mean volume cloud droplet radius, r_3, is explicitly calculated from the in-cloud liquid water content, l, and the cloud droplet number concentration, N:

$$r_3 = \left(\frac{l\,\rho_{\mathrm{air}}}{(4/3)\,\pi \rho_{\mathrm{water}} N} \right)^{1/3}, \quad (2)$$

but is a different measure of the size distribution than the effective droplet radius, r_e, which is defined as:

$$r_e = \frac{\int r^3 n(r)\,\mathrm{d}r}{\int r^2 n(r)\,\mathrm{d}r}. \quad (3)$$

However, simultaneous measurements of r_3 and r_e suggest a linear regression between the two radii for liquid clouds (Martin and Johnson, 1992) with:

$$r_e = 1.1\, r_3. \quad (4)$$

The combination of eqs. (2), (3) and (4) eventually ties r_e to the CDNC.

3. Description of the models

We use output from the MOGUNTIA chemical model as input for the LMD (Laboratoire de Météorologie Dynamique) and the ECHAM (European Centre for medium range weather forecast model, HAMburg version) GCMs.

3.1. The MOGUNTIA model

The MOGUNTIA model (Zimmermann, 1984, 1987) is an Eulerian chemical transport model, with a 10° resolution in latitude and longitude and 10 vertical layers. Wind, precipitation and temperature are prescribed from climatological monthly values. This model has been used by Langner and Rodhe (1991) and Langner et al. (1992) to investigate the tropospheric sulfur cycle. They considered three sulfur components: dimethylsulphide (DMS), SO_2 and aerosol sulfate (SO_4^{2-}). Sources were divided into anthropogenic and natural emissions (from oceans, plants, soils and volcanoes). The model was run twice, first with natural and anthropogenic sources (industrial case) and secondly with natural sources only (pre-industrial case) (cf. Table 2). The "standard oxidation rate" (see Langner and Rodhe, 1991) for in-cloud oxidation of SO_2 has been used in these simulations. This yields sulfate concentrations about 40% larger than for the "slow oxidation rate" which was used in previous studies (e.g., Jones et al., 1994). Note that we use three-dimensional distributions of the aerosol mass concentration whereas Jones et al. (1994) expanded half of the sulfate burden in the lowest 1.5 km of the atmosphere. Also, 90% of biomass burning emissions of SO_2 was considered as being anthropogenic. Soot and organic carbon particles were not included, although according to Penner et al. (1992) they also act as CCN and add to the forcing. The model has been compared to different sets of measurements (Langner and Rodhe, 1991; Langner et al., 1993). In general, there is a fair agreement between modelled and measured sulfate concentrations but observations are mostly located in and around polluted regions. However, the treatment of chemical processes and the estimates of the sources have to be improved in order to better simulate the seasonal variability. The model also seems to calculate too high concentrations of sulfate in the upper troposphere over the Pacific (Langner et al., 1993) but this is of little importance for this study since we are mainly interested in the lower troposphere. The model was integrated over 18 months and monthly-mean values of the aerosol mass fields were extracted from the last 12 months of integration. Fig. 2 shows the annually-averaged distribution of sulfate aerosol mixing ratio in the industrial and pre-industrial cases, respectively.

Table 2. *Emissions of sulfur components used in the chemical transport model calculations; unit: Tg S yr^{-1}*

Sources	Industrial case	Pre-industrial case
anthropogenic SO_2	66.5	0
anthropogenic SO_4^{2-}	3.5	0
biomass burning (SO_2)	2.5	0.25
volcanoes ($SO_2 + SO_4^{2-}$)	8.5	8.5
oceans (DMS)	16	16
soils and plants (DMS)	1	1

3.2. The LMD and ECHAM GCMs

Two climate models are used in the present study: the LMD and the ECHAM GCMs.

The LMD GCM has been described by Sadourny and Laval (1984). It is a grid-point model with 64 points evenly spaced in longitude, 50 points evenly spaced in sine of the latitude and 11 σ-levels. The version of the model used here takes into account the diurnal cycle.

The dynamics and part of the model physics of the ECHAM model have been adopted from the ECMWF model (Roeckner et al., 1992). Prognostic variables are vorticity, divergence, temperature, (logarithm of) surface pressure and the mass mixing ratios of water vapor and large-scale cloud water (liquid- and ice-phase together). The model equations are solved on 19 vertical levels in a hybrid pressure-sigma system by using

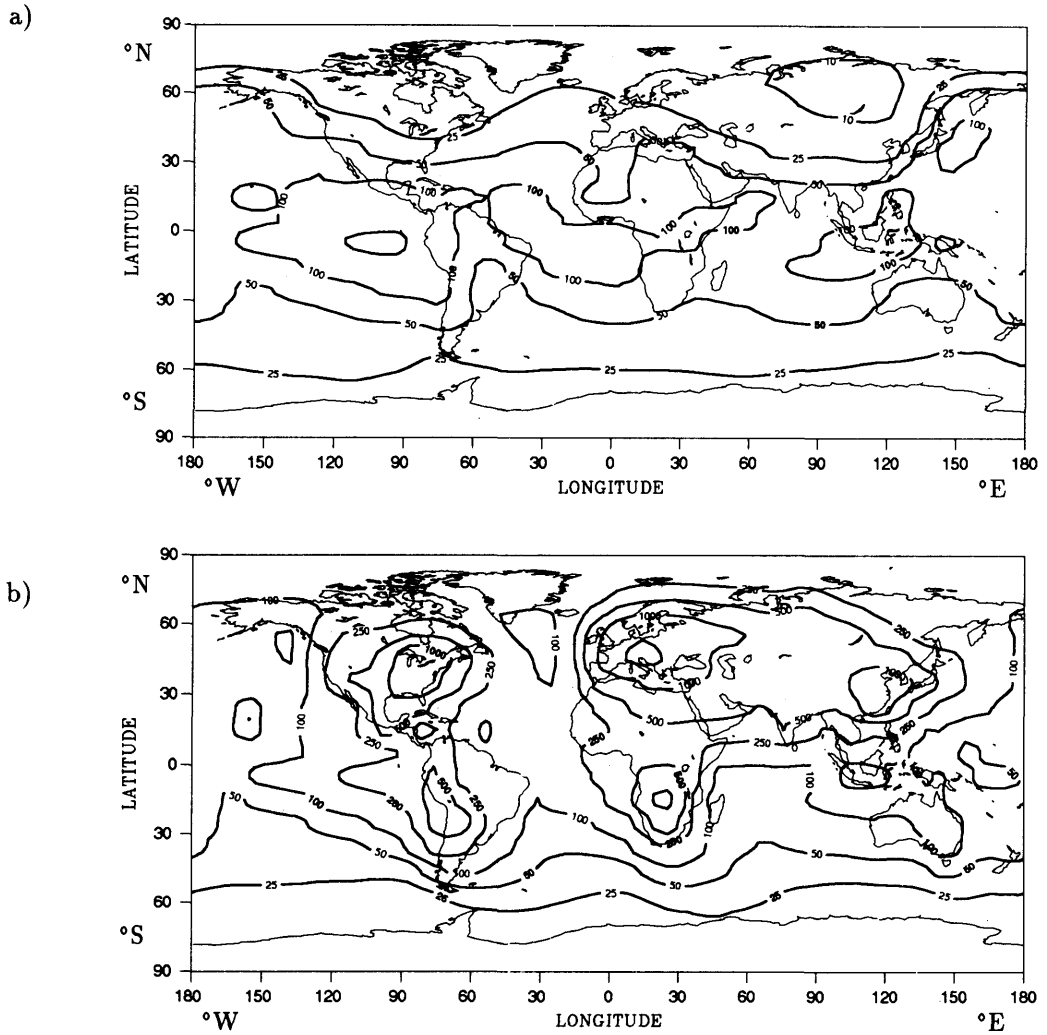

Fig. 2. Calculated annually-averaged distribution of SO_4^{2-} in the lowest level (1000–950 hPa) in (a) the pre-industrial case, and (b) the industrial case. Isolines are 25, 50, 100, 250, 1000, 2500 pptv. Adapted from Langner et al. (1992).

the spectral transform method with triangular truncation at wavenumber 21 (T21). Nonlinear terms and physical processes are evaluated at grid-points of a "Gaussian grid" providing a nominal resolution of $\sim 5.6° \times 5.6°$.

Both models have liquid water as a prognostic variable but the treatments of moist processes are quite different. In this version of the LMD GCM, we use the convective and the stratiform condensation schemes sequentially, and retain the convective cloud water in the atmosphere before entering the large-scale precipitation scheme. We have therefore complete detrainment of the convective cloud water in the stratiform clouds, or reevaporation of convective cloud water in an unsaturated environment. This is a crude representation of reality because convective cloud water might precipitate before being detrained into a stratiform cloud. However, the error introduced by the present treatment remains acceptable in terms of the global radiative fluxes as inferred from recent experiments. More sophisticated convective

schemes are required to handle these processes adequately. The stratiform condensation scheme is based on a simple statistical approach where a given subgrid-scale distribution of total (vapor and cloud) water is assumed (Le Treut and Li, 1991). The cloud fraction is defined as the part of the grid-box where the total water exceeds the water vapor mixing ratio at saturation. Condensation then occurs in the cloudy part and the cloud water content is computed as the difference between total water in the cloudy fraction of the grid-box and the water vapor mixing ratio at saturation. Precipitation is parameterized following Boucher et al. (1994) but CDNC, which is one of the parameters of the scheme, is prescribed here to a fixed value.

In the ECHAM model, the convection scheme is also called before the large-scale cloud scheme. In contrast to the LMD model, only the detrained fraction of convective cloud water is used as a source term in the large-scale cloud water equation. The stratiform cloud scheme is based on the work of Sundqvist (1978) and Roeckner et al. (1991). The fractional cloudiness is a nonlinear function of the relative humidity (Sundqvist et al., 1989) with thresholds depending on height and convective activity (Xu and Krueger, 1991). The cloud phases of droplets and ice crystals are separated diagnostically according to their temperature (Rockel et al., 1991). Rain is formed by autoconversion and accretion according to Sundqvist (1978) and Smith (1990). Gravitational settling of ice crystals is governed by the terminal velocity, which is parameterized in terms of ice water content (Heymsfield, 1977). Evaporation of precipitation below cloud base depends on the saturation deficit.

The same radiation code is used in both models. It is based on a two-stream method of the radiative transfer equations with six spectral intervals in the terrestrial infrared (Morcrette, 1989) and two in the solar part of the spectrum (0.25–0.68 and 0.68–4.0 μm) (Fouquart and Bonnel, 1980). However, shortwave cloud optical properties are computed differently in the two models.

Cloud optical depth (τ) is a weighted sum of τ_w and τ_c, the cloud optical depths for liquid and ice clouds:

$$\tau = x\,\tau_w + (1-x)\,\tau_c, \tag{5}$$

where x is the fraction of water that is liquid. It varies from 1 to 0 between 0 and -40°C in a linear way in the LMD GCM and in an exponential way in the ECHAM GCM (Rockel et al., 1991).

In the LMD GCM, cloud optical depth is:

$$\tau = x\,\frac{3}{2}\,\frac{W}{r_e} + (1-x)\,\frac{3}{2}\,\frac{W}{r_{ice}}, \tag{6}$$

where W is the cloud water path and r_{ice}, the equivalent effective radius for ice crystals, is set to 25 μm to account for the non-sphericity of ice crystals. In the ECHAM GCM, the single scattering properties of clouds are derived from Mie theory and the results fitted to the spectral resolution of the radiation model and formulated in terms of cloud droplet and ice crystal effective radii (Rockel et al., 1991). The cloud optical depth, which is different for the 2 spectral intervals, is given by:

$$\left.\begin{aligned}\tau_1 &= x\,1.87\,W\cdot r_e^{-1.08} \\ &\quad + (1-x)\,1.91\,W\cdot r_{ice}^{-1.03} \\ \tau_2 &= x\,1.97\,W\cdot r_e^{-1.08} \\ &\quad + (1-x)\,2.17\,W\cdot r_{ice}^{-1.06},\end{aligned}\right\} \tag{7}$$

where r_{ice} is a function of the ice water content.

The asymmetry factor (for liquid clouds), g, is a constant in each of the two spectral bands in the LMD GCM and has been computed using a high resolution spectral model:

$$\left.\begin{aligned}g_1 &= 0.865 \\ g_2 &= 0.910,\end{aligned}\right\} \tag{8}$$

whereas it is a function of the effective radius in the ECHAM model:

$$\left.\begin{aligned}g_1 &= 0.79 + 0.11\,\log r_e - 0.03(\log r_e)^2 \\ g_2 &= 0.79 - 0.04\,\log r_e + 0.19(\log r_e)^2 \\ &\quad - 0.08(\log r_e)^3.\end{aligned}\right\} \tag{9}$$

The single scattering albedo (for liquid clouds), ω, is an empirical function of cloud optical depth in the LMD GCM to account for the saturation of the liquid water absorption bands (Fouquart and Bonnel, 1980):

$$\left.\begin{aligned}\omega_1 &= 0.9999 - 5.0\cdot 10^{-4}\exp(-0.5\tau) \\ \omega_2 &= 0.9988 - 2.5\cdot 10^{-3}\exp(-0.05\tau),\end{aligned}\right\} \tag{10}$$

and again a function of the effective radius in the ECHAM model:

$$\left.\begin{aligned}\omega_1 &= 0.9999,\\ \omega_2 &= 0.986 + 0.014 \log r_e - 0.025(\log r_e)^2\\ &\quad + 0.006(\log r_e)^3.\end{aligned}\right\} \quad (11)$$

3.3. *Model experiments*

We consider that sulfate particles modify only the shortwave radiative properties of liquid clouds and the liquid-phase of mixed clouds. It is reasonable, in this context, to ignore changes in the longwave optical properties of liquid clouds, because most of them are thick enough to act as black bodies. We make a single 5-year experiment with both GCMs and compute diagnostically the shortwave radiative fluxes at each time-step. The calculations are made for droplet effective radius derived from each relationship and from both pre-industrial and present-day sulfate distributions. From now on, we refer to the experiments in accordance to the relationship used for the calculations (see Table 3). The experiments are so-called "forcing" experiments, where no feedbacks on the dynamics and physics are allowed: to advance from one time-step to the next one, we use the standard parameterization of the droplet effective radius in each model (not discussed here). The indirect effect is taken to be equal to the difference in shortwave radiative fluxes at the top of the atmosphere between present-day and pre-industrial conditions and is normalized by a factor that ensures that the simulated cloud radiative forcing (CRF) is equal to its ERBE value (Hartmann, 1993). This scaling is necessary because the simulated CRFs are different in the two models and depend also on the choice of the relationship. The scaling factor is ranging between 0.73 and 0.90 for the LMD GCM and between 0.93 and 1.08 for the ECHAM GCM. The different effective radii are computed with the same liquid water content. Although not well documented, the assumption that CDNC does not modify the liquid water content seems reasonable, since Leaitch et al. (1992b) did not find any correlation between CDNC and liquid water content. This approach is similar to that of Jones et al. (1994) and does not allow any feedbacks on cloud cover and precipitation efficiency, in contrast to the approach of Boucher and Rodhe (1994). These potential feedbacks are uncertain but may be substantial.

Table 3. *Table of experiments*

Exp.	Description	Eq.
A	mean regression lines for maritime, continental strat. and cum. clouds	eq. (A)
B	max. envelope	eq. (B)
C	min. envelope	eq. (C)
D	mean regression for all datasets	eq. (D)

4. Results

4.1. *Cloud droplet number concentration*

As shown in Fig. 3b, the distribution of CDNC for experiment A is primarily a reflection of the distribution of sulfate aerosol mass in the industrial case, with maxima over continents of the Northern Hemisphere.

The distribution of CDNC in the pre-industrial case (Fig. 3a) exhibits a land/sea contrast which does not show up in the sulfate mass distribution. This is because at low sulfate concentrations, the regression line for continental clouds predicts more cloud droplets than the one for maritime clouds. Although very difficult to verify, this feature seems reasonable because sulfate may not be the prevailing aerosol in the pre-industrial continental boundary layer; we might also expect the presence of a background concentration of CCN independent of the sulfate concentration. Moreover, it is legitimate to distinguish continental from maritime clouds since the relative importances of the processes governing the aerosol formation are different.

On the other side, the strong gradient in CDNC simulated near the coasts justify afterwards the use of relationship D which is unique for both maritime and continental clouds. This relationship has the further advantage that air masses being advected off the coasts do not change character when passing the coastline.

4.2. *Diagnostics of effective radii*

In Figs. 4, 5, we display 5-year zonal averages of the effective droplet radius for experiments A and D and in Table 4 the mean hemispheric effective

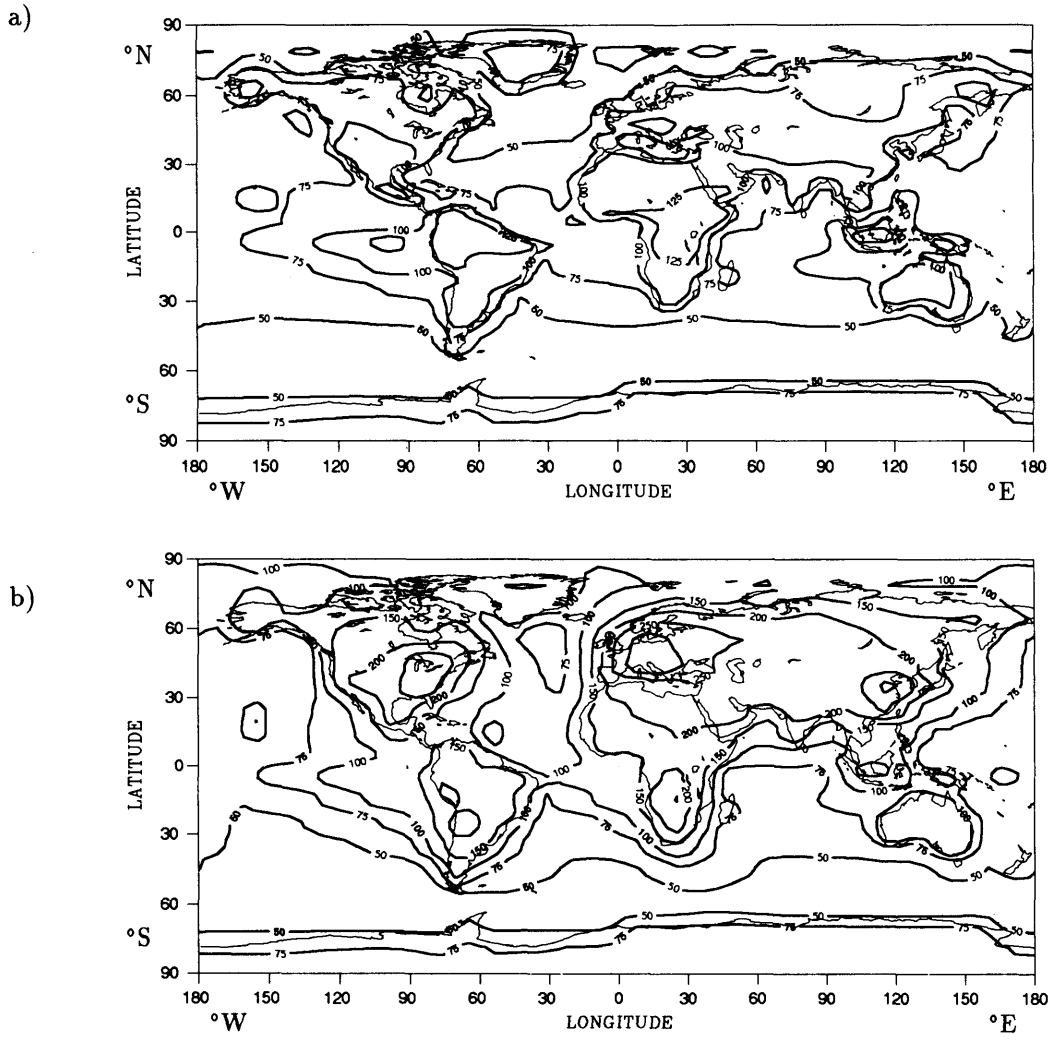

Fig. 3. Simulated distribution of annual mean cloud droplet number concentration (cm^{-3}) in the second layer (at about 950 hPa) for experiment A in (a) the pre-industrial, and (b) the industrial case. Over continents the CDNC is for stratiform clouds only.

radii for the different experiments. We compare our simulated effective radii to the measurements of Han et al. (1994) (see Fig. 6) who used an iterative algorithm to retrieve droplet effective radii of liquid clouds from ISCCP satellite data. The authors estimated that their results could be biased by 1 or 2 μm due to cirrus contamination or inappropriate treatment of the cloud element size distribution in a pixel. To make the comparison with the satellite data easier, we restrict ourselves to clouds with temperatures greater than 0°C and take the weighted average of cloud droplet radii over the fractional cover of low-level clouds. There are significant differences between the two models regarding the mean values of droplet radii and the shape of the latitudinal dependence, which illustrates the differences in the treatment of the cloud water budget. In particular, the simulated

Table 4. *Mean hemispheric effective radius; units: μm*

Experiment		Industrial case NH	Industrial case SH	Pre-industrial case NH	Pre-industrial case SH
A	ocean	9.3	10.1	10.3	10.4
LMD	land	8.0	8.7	9.8	9.6
A	ocean	8.3	8.9	9.4	9.2
ECHAM	land	4.9	5.4	5.8	5.9
B	ocean	6.6	7.6	7.8	7.9
LMD	land	5.9	6.7	8.0	7.7
B	ocean	6.2	7.0	7.5	7.4
ECHAM	land	4.0	4.8	5.5	5.6
C	ocean	14.6	15.0	15.3	15.1
LMD	land	10.2	10.7	11.1	11.1
C	ocean	12.5	12.8	13.2	13.0
ECHAM	land	5.9	6.4	6.5	6.7
D	ocean	8.2	8.8	8.9	9.0
LMD	land	8.0	9.1	11.0	10.6
D	ocean	7.3	7.7	8.1	7.9
ECHAM	land	5.6	6.7	7.7	7.8

droplet radii are too small in the ECHAM model compared to the satellite retrievals. It is also worth noting that the agreement between the two models is better for the difference plots (Figs. 4c, d and Figs. 5c, d).

Han et al. (1994) observed a significant land/sea contrast of 3.3 μm, droplets being smaller over the continents, but also a systematic difference between the two hemispheres, with larger droplets in clouds of the Southern Hemisphere. This hemispheric contrast of 0.7 μm could be due to anthropogenic aerosols. For experiment A, the land/sea contrast is simulated in both models (Figs. 4a, b), but is more pronounced in the ECHAM model (3.7 μm), than in the LMD GCM (1.6 μm). The large land/sea contrast in the ECHAM model is due to the fourfold effect of relationship A (which distinguishes continental from maritime clouds), higher sulfate loadings over continents, the special treatment of convective clouds over continents, and the model climatology (smaller liquid water contents in continental clouds compared to maritime clouds and to the LMD GCM). Droplets

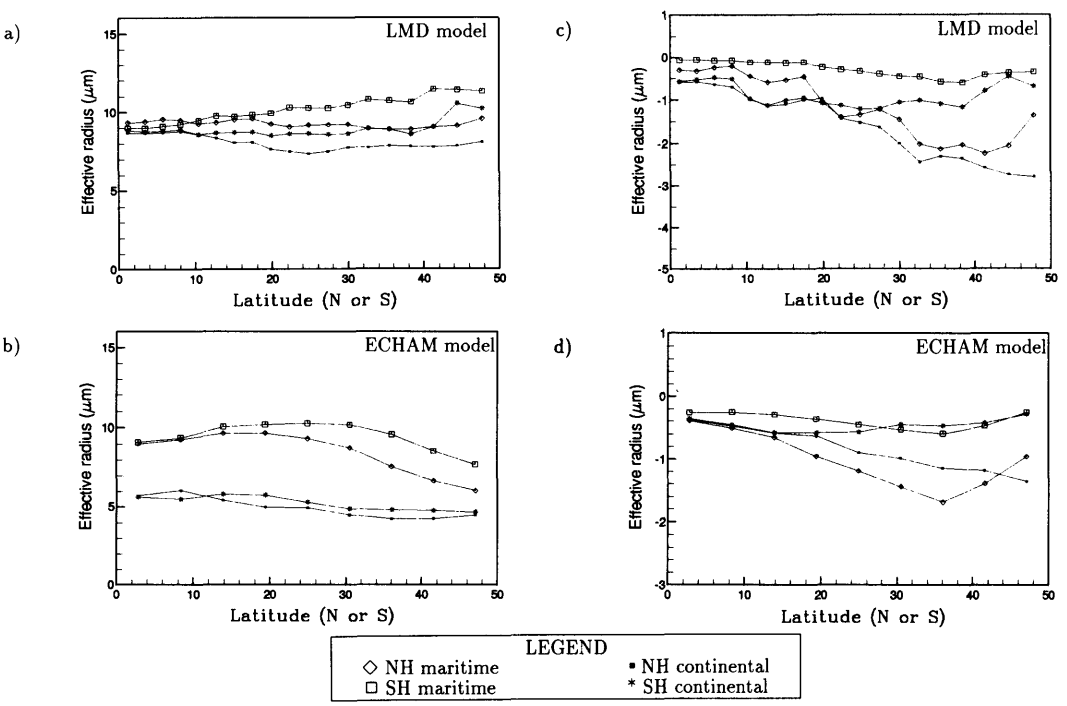

Fig. 4. Annual latitudinal averages of droplet effective radii simulated by (a) the LMD, and (b) the ECHAM GCMs for experiment A and for industrial conditions; difference in effective radii between the industrial and pre-industrial conditions for (c) the LMD, and (d) the ECHAM GCMs.

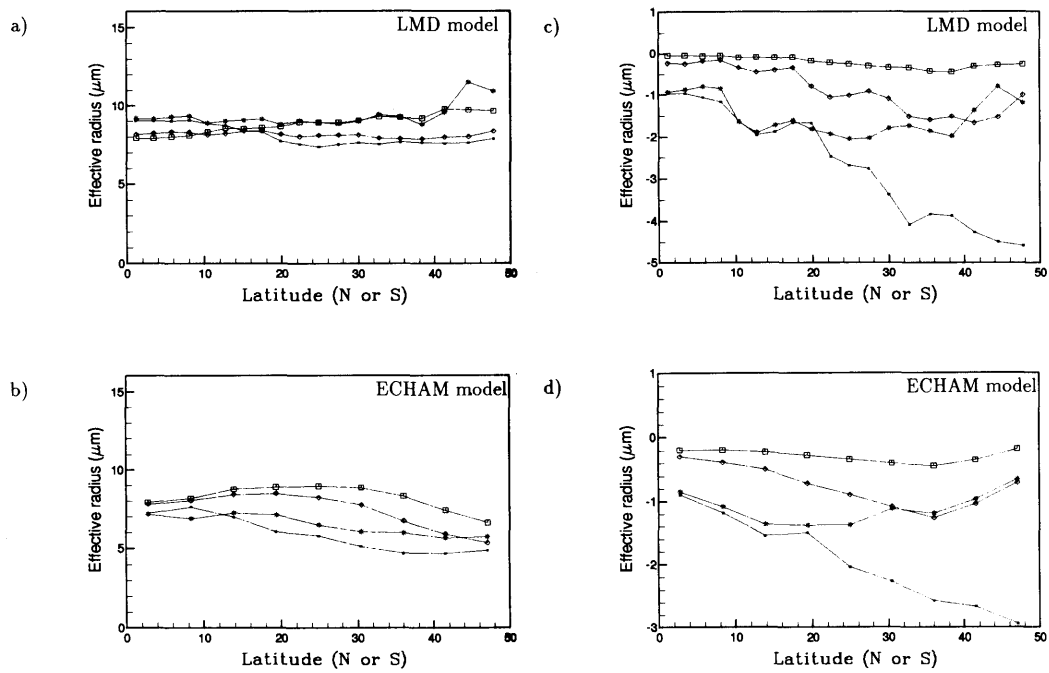

Fig. 5. Same as Fig. 4 but for experiment D.

in the Southern Hemisphere are 1.0 and 1.1 μm larger than in the Northern Hemisphere for the LMD and ECHAM GCMs, respectively. This hemispheric contrast drops to 0.1 and 0.4 μm in the pre-industrial case, whereas the land/sea contrast remains in both GCMs (Figs. 4c, d).

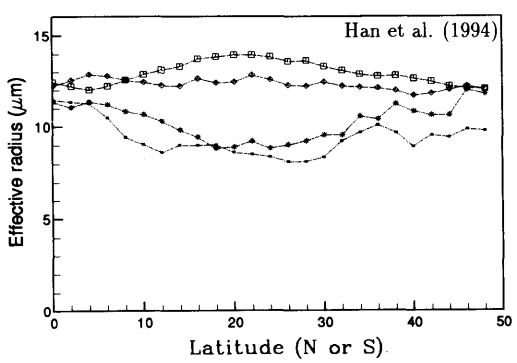

Fig. 6. Zonal means of satellite retrieved cloud droplet effective radius. From Han et al. (1994). Same legend as in Fig. 4.

There is a discrepancy between simulated and observed radii, which is common in both models: the maximum difference between maritime clouds of the Northern Hemisphere and Southern Hemisphere occur between 15° and 30° in the satellite data, but polewards of 40° in the GCMs. In both models, the maximum difference between pre-industrial and present-day conditions occur at mid-latitudes: at most 3 μm for Northern Hemisphere continents in LMD and 1.6 μm for Northern Hemisphere oceans in ECHAM.

In experiment D, with only one relationship for all clouds, there is no land/sea contrast in either model (Fig. 5a, b), but the hemispheric contrast remains, although slightly reduced. The difference between the industrial and pre-industrial conditions is more pronounced over the continents but less pronounced over the oceans, because the slope of the relationship is increased over continents and reduced over oceans.

4.3. Short-wave indirect aerosol forcing

The normalized, globally-averaged, indirect radiative forcing is found to be -1 W m^{-2} in both

Table 5. *Normalized SW indirect radiative forcings (see text); units: W m^{-2}*

Experiment		Normalized forcing NH	SH	global
A	LMD	−1.6	−0.4	−1.0
	ECHAM	−1.4	−0.6	−1.0
B	LMD	−2.2	−0.6	−1.4
	ECHAM	−2.1	−0.9	−1.5
C	LMD	−0.8	−0.2	−0.5
	ECHAM	−0.6	−0.3	−0.45
D	LMD	−1.7	−0.4	−1.05
	ECHAM	−1.6	−0.6	−1.1

models for relationship A. The computed forcing differs by less than 1% if we assume that the scavenging coefficient for sulfate is 100% (which has for consequence to shift relationship A for stratiform clouds towards lower sulfate concentrations). The forcing is larger in the Northern Hemisphere in both models but the hemispheric contrast is more pronounced in the LMD GCM (see Table 5). The maximum and minimum envelopes give an upper (-1.5 W m^{-2}) and a lower bound (-0.4 W m^{-2}) to the forcing. The simulated forcing is about the same in experiments D (-1.1 W m^{-2}) and A (-1.0 W m^{-2}), although the geographical distribution differs.

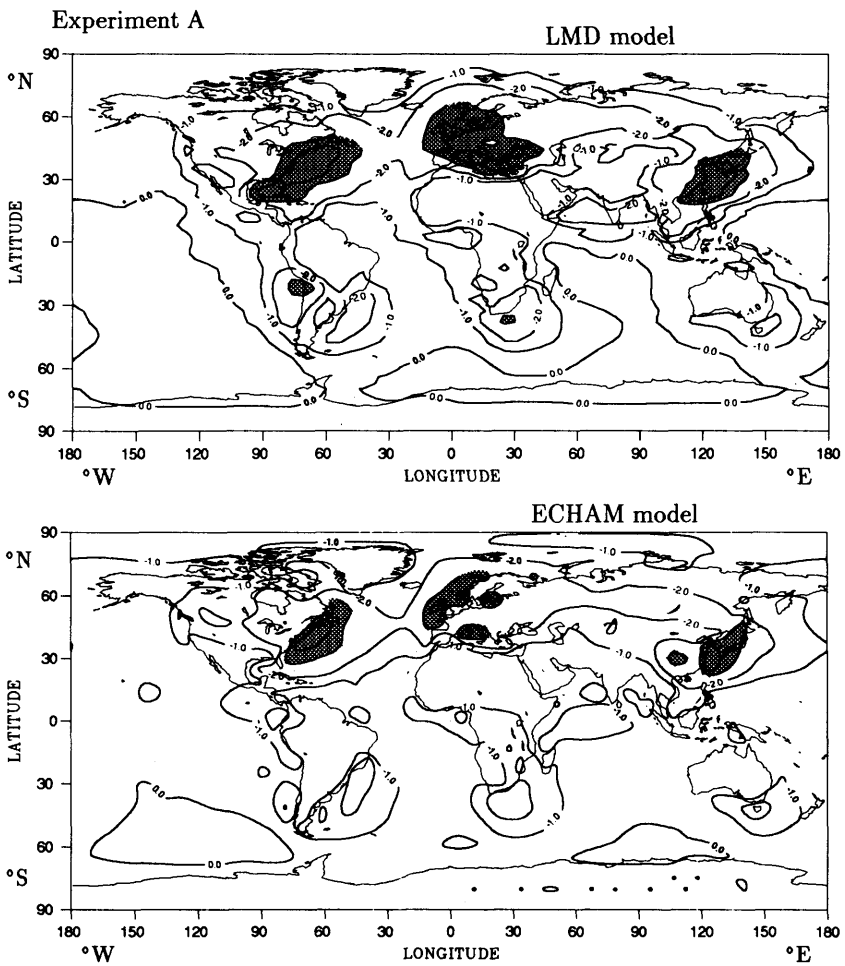

Fig. 7. Calculated loss of solar radiance (W m^{-2}) due to the indirect effect of sulfate aerosols for experiments A and D, and for both models. Regions of high forcing (lower than -4 W m^{-2}) are shaded.

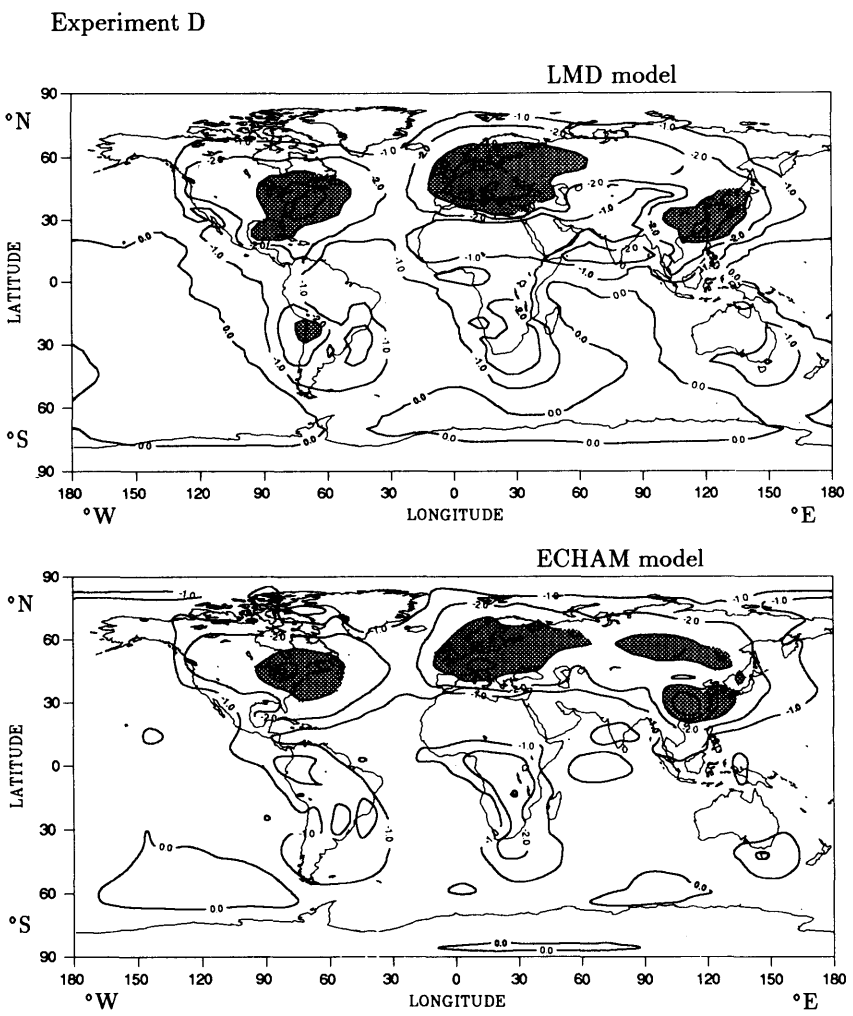

Fig. 7. (cont'd).

In experiment A, the largest forcing occurs off the coasts of the polluted regions (see Fig. 7a). As discussed above, this results from the steeper regression line used for maritime clouds than for continental clouds and also because large anthropogenic concentrations of sulfate can be found off the coasts, having a continental origin. The maximum value of forcing is larger in the LMD than in the ECHAM GCM. Differences occur off the west coasts of America and Africa, where ECHAM does not predict enough stratiform low-level clouds. The treatment of convective clouds in the LMD model tends to overpredict the amount of cloud in convectively active regions, which leads to higher values of the forcing in parts of the ITCZ. Other deviations in the forcing can be due to differences in cloud cover distribution, liquid water content and the treatment of shortwave optical properties in both models.

Contrarily, the forcing simulated in experiment D, where a single relationship is used, is largest over the continents of the Northern Hemisphere (see Fig. 7b). This is more in agreement with the results of Jones et al. (1994) and corresponds to the regions where the largest differences in sulfate mass concentration occur. The forcing remains

large over the Atlantic Ocean. The forcing in the Southern Hemisphere is 25% and 36% of the northern hemispheric value in the LMD and ECHAM models, respectively, whereas the change in sulfate aerosol in the Southern Hemisphere is only 16% that of the Northern Hemisphere. Cloud susceptibility is defined by Platnick and Twomey (1994) as the derivative of coud albedo with respect to CDNC for a given liquid water content. Clouds of the Southern Hemisphere are more susceptible than those of the Northern Hemisphere, because the CDNC is smaller in the Southern Hemisphere than in the Northern Hemisphere. Similar conclusions were reached by Platnick and Twomey (1994), Taylor and Mc Haffie (1994), and Jones et al. (1994).

The seasonal shortwave indirect aerosol forcing is shown in Fig. 8. The forcing is largest in the Northern Hemisphere, with a maximum in April in both models, whereas the change in sulfate aerosol is largest in the northern hemispheric winter. This is mostly due to the seasonal cycle of the insolation at mid-latitudes in the Northern Hemisphere. The maximum forcing in ECHAM follows the insolation thereby extending to the northern hemisphere high latitudes during the boreal summer, a feature that does not show up in the LMD model. This discrepancy (between the models) results from differences in the liquid water content, which may be underpredicted in the LMD model at high latitudes. Thus, a change in CDNC at higher liquid water content yields a large change in cloud albedo. The minimum occurs in November, revealing again the competition between decreasing insolation and increasing sulfate concentration during the period of July to December.

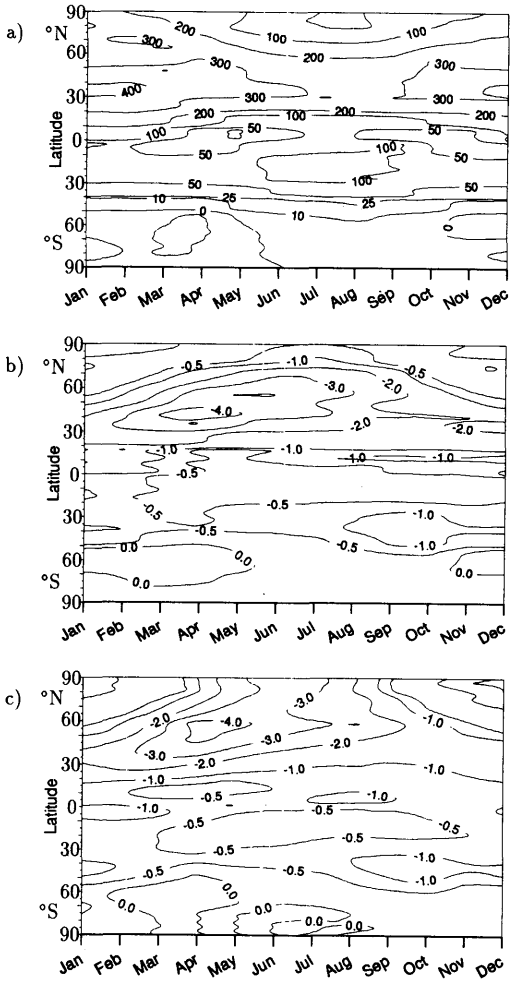

Fig. 8. Hovmöller diagram of (a) the anthropogenic sulfate aerosol concentration at the near-surface level (pptv), the SW aerosol indirect forcing ($W m^{-2}$) in (b) the LMD, and (c) the ECHAM GCMs.

5. Discussion

This modelling study suggests that the shortwave indirect radiative forcing could be of the same magnitude as that calculated for the direct effect (Charlson et al., 1991; Kiehl and Briegleb, 1993), but it has a much greater uncertainty. It is also consistent with the estimate provided by Jones et al. (1994) although their forcing is slightly higher (i.e., -1.3 W m^{-2}).

Kim and Cess (1993) analysed satellite-measured low-level cloud albedo in different latitude bands in both hemispheres and found evidences for an anthropogenic enhancement of cloud albedo over the east coasts of North America and China. The longitudinal extent of the anthropogenic influence is from 76° to about 65° W over the North Atlantic (latitude band 38°–43° N) and from 120° to 140° E over the North Pacific (latitude band 31°–39° N). Similarly, Falkowski et al. (1992) concluded that the influence of anthropogenic emissions on cloud albedo over the North Atlantic Ocean was limited to the east coast of the United States but their

study also suggests that natural processes could explain a large part of the variability of cloud albedo over this region. The influence of anthropogenic aerosols on coastal maritime clouds is also present in our model results, but its geographical extension is probably too large over the North Atlantic, which would produce an overestimate of the forcing.

Compared to the satellite data, the simulated contrast is too large in both models at mid-latitudes where the sulfate forcing is largest. Because this hemisperic contrast in cloud radii is thought to be due, at least in part, to anthropogenic aerosols, we believe that our forcing is likely to be an overestimate. There are two additional reasons why the forcing may be too large. First, in the ECHAM model, the simulated droplet radii, especially over land, are too small with respect to Han et al. (1994), thus tending to enhance the effect of CDNC on cloud albedo. Secondly, in the LMD GCM, the decrease in droplet radii from pre-industrial to present-day conditions is much larger than the hemispheric contrast.

Over Eastern North America, our estimate is larger than the one predicted from an elementary model by Leaitch et al. (1992b). These authors divided their data into polluted and clean-air subsets. If the CDNC of all clouds is increased from their median clean-air value of 160 cm^{-3} to their median value of all their data (250 cm^{-3}), the present climate forcing is estimated to be -2 to -3 $W m^{-2}$ over Eastern North America. In both GCMs the simulated CDNC increases from about 90 cm^{-3} to between 200–280 cm^{-3} for stratiform clouds, yielding a forcing between -2 and -4.5 $W m^{-2}$. This is in agreement with the fact that our natural CDNC for stratiform clouds is lower than the corresponding value of Leaitch et al. (160 cm^{-3}).

In view of the results presented above, we can now discuss the realism of the two relationships A and D, and whether maritime and continental clouds need to be distinguished or not. Generally speaking, the simulated droplet radii of experiment A show better agreement with the observed radii in respect to the land/sea contrast than experiment D. This supports the use of two relationships to describe maritime and continental clouds. On the other hand, air masses passing from land to ocean do not change character simply because they pass over the coastline. A smoother transition between land and ocean is needed rather than the discontinuity introduced by relationship A. The problem raised here is particularly crucial because anthropogenic sulfate mass is concentrated over continents and near coastlines. This suggests that, to model adequately the indirect aerosol effect, information about the time history of air masses is needed and that CCN number concentration should be a prognostic variable rather than diagnosed from the aerosol mass.

It is worth stressing that large uncertainties remain regarding the sulfate distribution (particularly in pre-industrial times). Also, the CDNC has been derived from the sulfate mass only, whereas the size distribution and the chemical composition of aerosols determine their CCN activity (Penner et al., 1994). Some mesoscale factors, not resolved by GCMs, give rise to natural variability of CDNC in real clouds, which makes it inadequate to represent CDNC by a single mean value. Other aerosol components can have a significant climate indirect effect as well, such as organic CCN (Novakov and Penner, 1993; Hegg et al., 1993) and biomass burning aerosols (Penner et al., 1992). The effect of entrainment/mixing processes in the clouds also have to be understood because they can lower the sensitivity of the CDNC to nss sulfate mass concentration (Novakov et al., 1994). A more precise understanding of the processes governing aerosol growth and droplet nucleation is needed before more certain statements can be made about the indirect effects of anthropogenic CCN on climate. This requires further measurements of sulfate mass and CDNC, but also more integrated approaches such as the so-called "closure experiments" proposed by Penner et al. (1994) and more comprehensive modelling approaches. The potential effect of anthropogenic aerosols on cloud lifetime may also be substantial (Parungo et al., 1994).

6. Summary and conclusions

The aim of this study has been to assess the indirect effect of anthropogenic sulfate aerosols on climate and the sensitivity of this effect to key modelling parameters. We have forced two GCMs with simulated fields of sulfate aerosol mass and utilized empirical relationships to relate sulfate

aerosol mass concentration and cloud droplet number concentration for pre-industrial and contemporary conditions. The indirect anthropogenic radiative forcing was defined as the difference in cloud radiative forcing between present-day and pre-industrial conditions. The agreement between the two climate models was good in terms of global averages of the simulated forcing but the geographical distribution and the simulated cloud droplet radii were different. These discrepancies arise from the different treatments of the cloud water budget equation and possibly from the different parameterizations of cloud optical properties. Although still very uncertain, the magnitude of the normalized indirect forcing is found to be about -1 W m^{-2} globally averaged in both GCMs, but it is very dependent on the assumed relationship between sulfate aerosol mass and cloud droplet number concentration. The uncertainty of this estimate, due to the somewhat arbitrary choice of the relationship, was estimated to be ± 0.5 W m^{-2} on the basis of two simulations where we consider a maximum and a minimum envelope of the available data. The total uncertainty of the forcing still cannot be assessed because we are lacking a quantitative knowledge of the processes leading to the formation of CCN and the nucleation of cloud droplets but it is certainly greater than the uncertainty estimated here on the basis of different sulfate mass to CDNC relationships (e.g., ± 0.5 W m^{-2}). Comparisons of our model results with satellite retrieval of cloud droplet radii (Han et al., 1994) indicate that the forcing we have obtained may be an overestimate. Also, if sulfate mass concentration is used as a surrogate for cloud droplet number concentration, a distinction should be made between maritime and continental clouds.

7. Acknowledgments

We would like to thank Ulf Hansson for having provided the data from the MOGUNTIA model, Henning Rodhe, Erich Roeckner, Hans Feichter and Hervé Le Treut for helpful advice. Computer time for numerical experiments at the LMD was provided by IDRIS (Institut du Développement et des Ressources en Informatique Scientifique). Olivier Boucher would like to acknowledge the Department of Meteorology, Stockholm University for its hospitality and the Swedish Institute for support.

REFERENCES

Ackerman, A. S., Toon, O. B. and Hobbs, P. V. 1994. Reassessing the dependence of cloud condensation nucleus concentration on formation rate. *Science* **367**, 445–447.

Albrecht, B. A. 1989. Aerosols, cloud microphysics, and fractional cloudiness. *Science* **245**, 1227–1230.

Albrecht, B. A., Randall, D. A. and Nicholls, S. 1988. Observations of marine stratocumulus clouds during FIRE. *Bull. Am. Meteor. Soc.* **69**, 618–626.

Anderson, T. L., Covert, D. S. and Charlson, R. 1994. Cloud droplet number studies with a counterflow virtual impactor. *J. Geophys. Res.* **99**, 8249–8256.

Berresheim, H., Eisele, F. L., Tanner, D. J., McInnes, L. M., Ramsey-Bell, D. C. and Covert, D. S. 1993. Atmospheric sulfur chemistry and cloud condensation nuclei (CCN) concentrations over the Northeastern Pacific coast. *J. Geophys. Res.* **98**, 12701–12711.

Boucher, O. and Rodhe, H. 1994. The sulfate-CCN-cloud albedo effect: a sensitivity study, *Report CM-83*, 20 pp. Department of Meteorology, Stockholm University, Sweden.

Boucher, O., Le Treut, H. and Baker, M. B. 1994. Sensitivity of a GCM to changes in cloud droplet concentration. In: *Preprints of the AMS 8th Conference on Atmospheric radiation*, 558–560. Nashville, Tennessee.

Charlson, R. J. 1992. Gas-to-particle conversion and CCN production. In: *International Symposium on Dimethylsulphide: oceans, atmosphere and climate*, 275–286. G. Restelli and G. Angeletti (eds.), Kluwer Academic Publishers, Boston.

Charlson, R. J., Langner, J. and Rodhe, H. 1990. Sulphate aerosol and climate. *Nature* **348**, 22.

Charlson, R. J., Langner, J., Rodhe, H., Levoy, C. B. and Warren, S. G. 1991. Perturbation of the northern hemisphere radiative balance by backscattering from anthropogenic sulfate aerosols. *Tellus* **43AB**, 152–163.

Charlson, R. J., Schwartz, S. E., Hales, J. M., Cess, R. D., Coakley, J. A., Hansen, J. E. and Hofmann, D. J. 1992. Climate forcing by anthropogenic aerosols. *Science* **255**, 423–430.

Chuang, C. C., Penner, J. E., Taylor, K. E. and Walton, J. J. 1994. Climate effects of anthropogenic sulfate:

Simulations from a coupled chemistry/climate model. In: *Preprints of the AMS Conference on Atmospheric chemistry*, 170–174. Nashville, Tennessee.

Clarke, A. D. 1992. Atmospheric nuclei in the remote free-troposphere. *J. Atmos. Chem.* **14**, 479–488.

Coakley, J. A., Bernstein, R. L. and Durkee, P. A. 1987. Effect of ship-stack effluents on cloud reflectivity. *Science* **237**, 1020–1022.

Falkowski, P. G., Kim, Y., Kolber, Z., Wilson, C., Wirick, C. and Cess, R. 1992. Natural versus anthropogenic factors affecting low-level cloud albedo over the North Atlantic. *Science* **256**, 1311–1313.

Fouquart, Y. and Bonnel, B. 1980. Computations of solar heating of the Earth's atmosphere: a new parameterization. *Beitr. Phys. Atmos.* **53**, 35–62.

Fouquart, Y. and Isaka, H. 1992. Sulfur emission, CCN, clouds and climate: a review. *Ann. Geophysicae* **10**, 462–471.

Gillani, N. V., Daum, P. H., Schwartz, S. E., Leaitch, W. R., Strapp, J. W. and Isaac, G. A. 1992. Fractional activation of accumulation-mode particles in warm continental stratiform clouds. In: *Precipitation scavenging and atmosphere-surface exchange*, vol. **1**, pp. 345–358. S. E. Schwartz and W. G. N. Slinn (eds.). Hemisphere Publishing Corporation.

Graßl, H. 1988. What are the radiative and climatic consequences of the changing concentration of atmospheric aerosol particles? In: *The changing atmosphere, 187–199*. F. S. Rowland and I. S. A. Isaksen (eds.). John Wiley & Sons.

Hallberg, A. 1994. *Aerosol particle properties influencing cloud droplet nucleation*, Ph.D. thesis. Paper no. IV. University of Stockholm, Sweden.

Hallberg, A., Ogren, J. A., Noone, K. J., Okada, K., Heintzenberg, J. and Svenningsson, I. B. 1995. The influence of aerosol particle composition on cloud droplet formation. *J. Atmos. Chem.* **19**, in press.

Han, Q., Rossow, W. B. and Lacis, A. A. 1994. Near-global survey of effective droplet radii in liquid water clouds using ISCCP data. *J. Climate* **7**, 465–497.

Hartmann, D. L. 1993. Radiative effects of clouds on Earth's climate. In: *Aerosol-cloud-climate interactions*, 151–173, vol. **54** of *International Geophysical Series*, P. V. Hobbs (ed.). Academic Press.

Hegg, D. A. 1994. The cloud condensation nucleus-sulfate mass relationship and cloud albedo. *J. Geophys. Res.*, in press.

Hegg, D. A. and Hobbs, P. V. 1988. Comparisons of sulfate and nitrate production in clouds on the Mid-Atlantic and Pacific northwest coasts of the United States. *J. Atmos. Chem.* **7**, 325–333.

Hegg, D. A., Hobbs, P. V. and Radke, L. F. 1980. Observations of the modification of cloud condensation nuclei in wave clouds. *J. Rech. Atmos.* **14**, 217–222.

Hegg, D. A., Hobbs, P. V. and Radke, L. F. 1984. Measurements of the scavenging of sulfate and nitrate in clouds. *Atmos. Env.* **18**, 1939–1946.

Hegg, D. A., Ferek, R. J. and Hobbs, P. V. 1993. Light scattering and cloud condensation nucleus activity of sulfate aerosol measured over the Northeast Atlantic Ocean. *J. Geophys. Res.* **98**, 14887–14894.

Heymsfield, A. J. 1977. Precipitation development in stratiform ice clouds: A microphysical and dynamical study. *J. Atmos. Sci.* **34**, 367–381.

Hobbs, P. V. 1993. Aerosol-cloud interactions. In: *Aerosol-cloud-climate interactions*, 33–73, vol. **54** of *International Geophysical Series*, P. V. Hobbs (ed.). Academic Press.

Hoppel, W. A., Frick, F. M. and Larson, R. E. 1986. Effect of nonprecipitating clouds on the aerosol size distribution in the marine boundary layer. *Geophys. Res. Lett.* **13**, 125–128.

Hoppel, W. A., Fitzgerald, J. W., Frick, G. M., Larson, R. E. and Mack, E. J. 1990. Aerosol size distributions and optical properties found in the marine boundary layer over the Atlantic Ocean. *J. Geophys. Res.* **95**, 3659–3686.

IPCC, 1992. *Climate Change 1992: The Supplementary Report to the IPCC Scientific Assessment*, J. T. Houghton, B. A. Callander and S. K. Varney (eds.). Cambridge University Press, United Kingdom.

Jones, A., Roberts, D. L. and Slingo, A. 1994. A climate model study of the indirect radiative forcing by anthropogenic sulphate aerosols. *Nature* **370**, 450–453.

Kaufman, Y. J. and Tanré, D. 1994. Effect of variations in supersaturation on the formation of cloud condensation nuclei. *Nature* **369**, 45–48.

Kiehl, J. T. and Briegleb, B. P. 1993. The relative roles of sulfate aerosols and greenhouse gases in climate forcing. *Science* **260**, 311–314.

Kim, Y. and Cess, R. D. 1993. Effect of anthropogenic sulfate aerosols on low-level cloud albedo over oceans. *J. Geophys. Res.* **98**, 14883–14885.

King, M. D., Radke, L. F. and Hobbs, P. V. 1993. Optical properties of marine stratocumulus clouds modified by ships. *J. Geophys. Res.* **98**, 2729–2739.

Langner, J. and Rodhe, H. 1991. A global three-dimensional model of the tropospheric sulfur cycle. *J. Atmos. Chem.* **13**, 225–263.

Langner, J., Rodhe, H., Crutzen, P. J. and Zimmermann, P. 1992. Anthropogenic influence of the distribution of tropospheric sulphate aerosol. *Nature* **359**, 712–716.

Langner, J., Bates, T., Charlson, R. J., Clarke, A. D., Durkee, P. A., Heintzenberg, J., Hofmann, D. J., Huebert, B., Leck, C., Lelieveld, J., Ogren, J. A., Prospero, J., Quinn, P. K., Rodhe, H. and Ryaboshapko, A. G. 1993. The global atmospheric sulfur cycle: An evaluation of model predictions and observations, *Report CM-81*, 28 pp. Department of Meteorology, Stockholm University, Sweden.

Leaitch, W. R. and Isaac, G. A. 1994. On the relationship between sulfate and cloud droplet number concentrations. *J. Climate* **7**, 206–212.

Leaitch, W. R., Isaac, G. A., Strapp, J. W., Banic, C. M. and Wiebe, H. A. 1992a. Concentrations of major ions in Eastern North American cloud water and their control of cloud droplet number concentrations. In: *Precipitation scavenging and atmosphere-surface*

exchange, vol. **1**, pp. 333–343, S. E. Schwartz and W. G. N. Slinn (eds.). Hemisphere Publishing Corporation.

Leaitch, W. R., Isaac, G. A., Strapp, J. W., Banic, C. M. and Wiebe, H. A. 1992b. The relationship between cloud droplet number concentrations and anthropogenic pollution: observations and climatic implications. *J. Geophys. Res.* **97**, 2463–2474.

Le Treut, H. and Li, Z. X. 1991. Sensitivity of an atmospheric general circulation model to prescribed SST changes: Feedback effects associated with the simulation of cloud optical properties. *Climate Dynam.* **5**, 175–187.

Martin, G. M. and Johnson, D. W. 1992. The measurements and parametrisation of effective radius of droplets in stratocumulus clouds. In: *Proceedings of the 11th International Conference on Clouds and precipitation*, vol. **1**, pp. 158–161. Montréal, Canada.

Morcrette, J. J. 1989. Description of the radiative scheme in the ECMWF model. *Technical Report no. 165*, 26 pp., ECMWF, Reading, United Kingdom.

Novakov, T. and Penner, J. E. 1993. Large contribution of organic aerosols to cloud-condensation-nuclei concentrations. *Nature* **365**, 823–826.

Novakov, T., Riviera-Carpio, C., Penner, J. E. and Rogers, C. F. 1994. The effect of anthropogenic sulfate aerosols on marine cloud droplet concentration. *Tellus* **46B**, 132–141.

Parungo, F., Boatman, J. F., Sievering, H., Wilkison, S. W. and Hicks, B. B. 1994. Trends in global marine cloudiness and anthropogenic sulfur. *J. Climate* **7**, 434–440.

Penner, J. E., Dickinson, R. E. and O'Neill, C. A. 1992. Effects of aerosol from biomass burning on the global radiation budget. *Science* **256**, 1432–1434.

Penner, J. E., Charlson, R. J., Hales, J. M., Laulainen, N. S., Leifer, R., Novakov, T., Ogren, J., Radke, L. F., Schwartz, S. E. and Travis, L. 1994. Quantifying and minimizing uncertainty of climate forcing by anthropogenic aerosols. *Bull. Am. Met. Soc.* **75**, 375–400.

Platnick, S. and Twomey, S. 1994. Determining the susceptibility of cloud albedo to changes in droplet concentration with the advanced very high resolution radiometer. *J. Appl. Meteor.* **33**, 334–347.

Quinn, P. K., Covert, D. S., Bates, T. S., Kapustin, V. N., Ramsey-Bell, D. C. and McInnes, L. M. 1993. Dimethylsulfide/cloud condensation nuclei/climate system: relevant size-resolved measurements of the chemical and physical properties of the atmospheric aerosol particles. *J. Geophys. Res.* **98**, 10411–10427.

Radke, L. F., Coakley, J. A. and King, M. D. 1989. Direct and remote sensing observations of the effects of ships on clouds. *Science* **246**, 1146–1148.

Rockel, B., Raschkle, E. and Weyers, B. 1991. A parameterization of broad band radiative transfer properties of water, ice and mixed clouds. *Beitr. Phys. Atmos.* **64**, 1–12.

Roeckner, E., Rieland, M. and Keup, E. 1991. Modelling of clouds and radiation in the ECHAM model. *ECMWF/WCRP Workshop on Clouds, radiative transfer and the hydrological cycle, 199–222.* ECMWF, Reading, United Kingdom.

Roeckner, E., Arpe, K., Bengtsson, L., Brinkop, S., Dümenil, L., Esch, M., Kirk, E., Lunkeit, F., Ponater, M., Rockel, B., Sausen, R., Schlese, U., Schubert, S. and Windelband, M. 1992. Simulation of the present-day climate with the ECHAM model: Impact of model physics and resolution. *Report no. 93*, 172 pp. Max-Planck-Institut für Meteorologie, Germany.

Sadourny, R. and Laval, K. 1984. January and July performance of the LMD general circulation model. In: *New perspectives in climate modelling*, A. Berger and C. Nicolis (eds.). Elsevier, Amsterdam.

Schlesinger, M. E., Jiang, X. and Charlson, R. J. 1992. Implication of anthropogenic atmospheric sulphate for the sensitivity of the climate system. In: *Climate change and energy policy*, 75–108, L. Rosen and R. Glasser (eds.). American Institute of Physics, New York.

Schwartz, S. E. 1988. Are global cloud albedo and climate controlled by marine phytoplankton? *Nature* **336**, 441–445.

Sievering, H., Van Valin, C. C., Barrett, E. W. and Pueschel, R. F. 1984. Cloud scavenging of aerosol sulfur. Two case studies. *Atmos. Env.* **18**, 2685–2690.

Smith, R. N. B. 1990. A scheme for predicting layer clouds and their water content in a general circulation model. *Quart. J. R. Meteor. Soc.* **116**, 435–460.

Sundqvist, H. 1978. A parameterization scheme for non-convective condensation including prediction of cloud water content. *Quart. J. R. Meteor. Soc.* **104**, 677–690.

Sundqvist, H., Berge, E. and Kristjánsson, J. E. 1989. Condensation and cloud parameterization studies with a mesoscale numerical weather prediction model. *Monthly Wea. Rev.* **117**, 1641–1657.

Taylor, J. P. and Mc Haffie, A. 1994. Measurements of cloud susceptibility. *J. Atmos. Sci.* **51**, 1298–1306.

Taylor, K. E. and Penner, J. E. 1994. Response of the climate system to atmospheric aerosols and greenhouse gases. *Nature* **369**, 734–737.

ten Brink, H. M., Schwartz, S. E. and Daum, P. H. 1987. Efficient scavenging of aerosol sulfate by liquid-water clouds. *Atmos. Env.* **21**, 2035–2052.

Twomey, S. 1959. The nuclei of natural cloud formation, Part II: The supersaturation in natural clouds and the variation of cloud droplet concentration. *Geofis. Pura Appl.* **43**, 243–249.

Twomey, S. 1974. Pollution and the planetary albedo. *Atmos. Env.* **8**, 1251–1256.

Twomey, S. A., Piepgrass, M. and Wolfe, T. 1984. An assessment of the impact of pollution on global cloud albedo. *Tellus* **36B**, 356–366.

Wigley, T. M. L. 1989. Possible climate change due to SO_2-derived cloud condensation nuclei. *Nature* **339**, 365–367.

Xu, K. M. and Krueger, S. K. 1991. Evaluation of cloudi-

ness parameterizations using a cumulus ensemble model. *Month. Wea. Rev.* **119**, 342–367.

Zimmermann, P. H. 1984. *Ein dreidimensionales numerisches Transportmodell für atmosphärische Spürenstoffe*. Ph.D. thesis, 160 pp., University of Mainz, Germany.

Zimmermann, P. H. 1987. MOGUNTIA: A handy global tracer model. In: *Proceedings of the 16th NATO/CCMS International Technical Meeting on Air pollution modeling and its application*, 593–608. D. Reidel, Dordrecht, Lindau, Germany.